

SCIENTIFIC REPORTS



OPEN

Superconductivity Bordering Rashba Type Topological Transition

M. L. Jin¹, F. Sun^{1,5}, L. Y. Xing¹, S. J. Zhang¹, S. M. Feng¹, P. P. Kong¹, W. M. Li¹, X. C. Wang¹, J. L. Zhu³, Y. W. Long¹, H. Y. Bai¹, C. Z. Gu¹, R. C. Yu¹, W. G. Yang^{4,5}, G. Y. Shen⁴, Y. S. Zhao^{1,3}, H. K. Mao^{4,5} & C. Q. Jin^{1,2,6}

Received: 24 October 2016

Accepted: 24 November 2016

Published: 04 January 2017

Strong spin orbital interaction (SOI) can induce unique quantum phenomena such as topological insulators, the Rashba effect, or p-wave superconductivity. Combining these three quantum phenomena into a single compound has important scientific implications. Here we report experimental observations of consecutive quantum phase transitions from a Rashba type topological trivial phase to topological insulator state then further proceeding to superconductivity in a SOI compound BiTeI tuned via pressures. The electrical resistivity measurement with V shape change signals the transition from a Rashba type topological trivial to a topological insulator phase at 2 GPa, which is caused by an energy gap close then reopen with band inverse. Superconducting transition appears at 8 GPa with a critical temperature T_c of 5.3 K. Structure refinements indicate that the consecutive phase transitions are correlated to the changes in the Bi–Te bond and bond angle as function of pressures. The Hall Effect measurements reveal an intimate relationship between superconductivity and the unusual change in carrier density that points to possible unconventional superconductivity.

Studies on the systems of strong spin orbital interactions (SOI), which play important roles in forming novel quantum states, intensively grown^{1–8}. A classical SOI phenomenon is the Rashba effect, which lifts the electron spin degeneracy with broken inversion symmetry^{9,10}. The Rashba effect is a momentum dependent splitting of spin bands in a no-centrosymmetric system. Other classical examples of SOI include topological quantum states such as topological insulators (TIs), wherein the bulk insulator state coexists with the robust metal edge (surface) state protected by topological invariance. The evolution of the Rashba system into a TI can provide an effective pathway to understand the mechanisms of these novel quantum states and their intrinsic connections, as well as provide opportunities for spintronic applications¹¹. More importantly, SOI phenomena such as TIs or the Rashba effect can be utilized to realize a p-wave superconductor^{3,12}. Similar to TIs, topological superconductors are expected to have gapless edge (or surface) states that can host long sought elusive Majorana fermions. Such unconventional superconductors are potentially important for new quantum computers^{7,8}.

Rashba polar semiconductor BiTeI hosts the largest known spin split band from its bulk polar atomic configuration⁹ with a Rashba parameter of 3.85 eVÅ at ambient conditions. It was recently theoretically predicated that BiTeI can be transformed from a topological normal state into a topological no trivial insulator by band inverse at high pressures¹⁰. The prediction received immediate experiments follow-up through observation of band close up then reopen & inverse as detected by IR spectroscopy¹³. High pressure can be a powerful method to generate new quantum states since it perishes the by products such as disorders or impurities introduced by chemical doping. Transport measurements at high pressures are especially effective in unveiling quantum state evolution in the SOI system since the TI compounds of Bi₂Te₃¹⁴, Sb₂Te₃¹⁵, or Bi₂Se₃¹⁶ become superconductive at high pressures.

This paper reports on the discovery of superconductivity in BiTeI induced by pressure that borders the transition from a Rashba type topological trivial state to a topological insulator state. Structure evolutions, including local structure distortion at high pressures, are investigated by Raman spectroscopy in conjunction with high pressure synchrotron X-ray diffraction.

¹Beijing National Laboratory for Condensed Matter Physics and Institute of Physics, Chinese Academy of Sciences, Beijing 100190, China. ²Collaborative Innovation Center of Quantum Matters, Beijing, China. ³HIPSEC, Department of Physics and Astronomy, University of Nevada at Las Vegas, Las Vegas, NV 89154-4002, USA. ⁴High Pressure Synergetic Consortium (HPSynC) & High Pressure Collaborative Access Team (HPCAT), Geophysical Laboratory, Carnegie Institution of Washington, Argonne, Illinois 60439, USA. ⁵Center for High Pressure Science & Technology Advanced Research (HPSTAR), Shanghai, China. ⁶School of Physical Sciences, University of Chinese Academy of Sciences, Beijing 100190, China. Correspondence and requests for materials should be addressed to C.Q.J. (email: Jin@iphy.ac.cn)

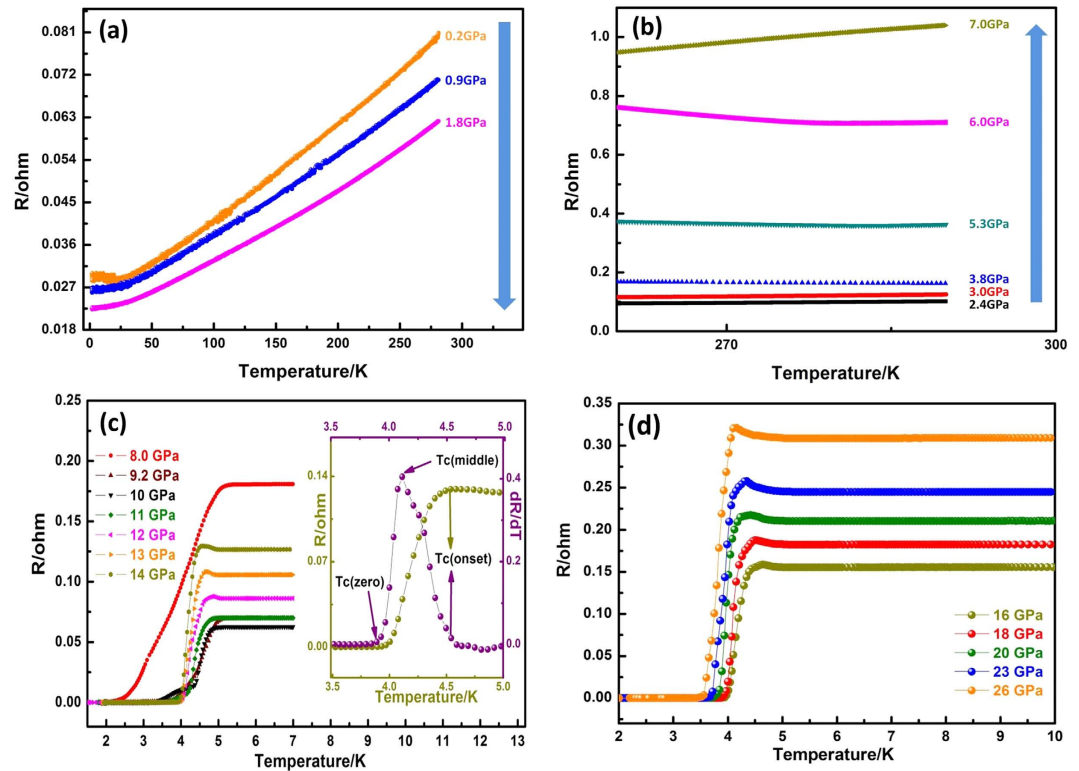


Figure 1. (a,b) Resistance of the BiTeI single crystal as function of temperature in the low pressure phase shows the topological quantum phase transition at ~ 2 GPa; (c,d) Resistance of the BiTeI single crystal as function of temperature in the high pressure range of 7 GPa to 26 GPa, which shows superconductivity at 5.3 K at 8.0 GPa. The inset of (c) is an enlargement of resistance versus temperature around the superconducting region at 14 GPa; the differential of resistance over temperature (dR/dT) shows the onset, middle, and zero transition temperatures, respectively.

Results and Discussion

High-pressure electrical transport properties of BiTeI single crystal. The ambient phase of BiTeI crystallizes into a non-centrosymmetric layered structure of the trigonal space group $P3m1$ with lattice parameters of $a = 4.3392 \text{ \AA}$ and $c = 6.854 \text{ \AA}$ ^{10,17}. Figure 1 shows the resistance evolution of the BiTeI single crystal as functions of pressure and temperature. The low resistance of the BiTeI crystal is generally caused by additional conductivity by certain defects mentioned in ref. 9. The BiTeI crystal resistance decreases with pressure in the region lower than 2 GPa as shown in Fig. 1(a). However, the resistance increases to a maximum with pressure at ~ 7 GPa upon crossing the critical pressure^{10,13} of ~ 2 GPa as shown in Fig. 1(b). When the pressure reaches above 8 GPa, superconductivity appears with an onset superconducting transition temperature $T_C^{(\text{onset})}$ of 5.3 K, where the value of T_C is defined using the method¹⁴ based on the differential of resistance over temperature as shown in the inset of Fig. 1(c). The $T_C^{(\text{onset})}$ value decreased to 4.5 K at 14 GPa with a rate $dT_C/dP = -0.14 \text{ K/GPa}$ and then reached approximately 4.1 K with a non-linear decrease as shown in Fig. 1(c) and 1(d), respectively.

Figure 2 shows the resistivity of the BiTeI single crystal at 280 K as function of pressures. The resistance decreases with pressure as a result of the energy band gap changes that narrows to a critical pressure (P_C) of ~ 2 GPa where the gap closes in the Rashba phase. Upon crossing the P_C , the inversion and opening up of the Bi 6_{pz} orbital and Te $I-5pz$ orbitals leads to the semiconducting behavior as shown in Fig. 1(b). The emergence of the semiconducting state, which comes from the conduction and valence band reconstruction, is the feature of the band gap reopening¹⁰. This phenomenon results in a V shape change in resistivity across P_C as shown in Fig. 2.

The superconductivity nature in the BiTeI single crystal was validated by the ac magnetic susceptibility measurement that results in transition with T_C at ~ 5 K that is similar to the conductivity measurements as shown in Fig. 3(a). Figure 3(b,c) shows superconducting transition as a function of the external magnetic field H perpendicular to the ab plane of the BiTeI single crystal. T_C decreases with the applied magnetic field H . The change in T_C with H is shown in Fig. 3(d). Using the Werthdamer–Helfand–Hohenberg formula¹⁸ of $H_{c2}(0) = -0.691T_C \times [dH_{c2}(T)/dT]_{T=T_C}$, the upper critical field H_{c2} was estimated to be 2.9 T and 2.8 T at 14 GPa and 26 GPa, respectively, for the magnetic H perpendicular to ab plane, which are comparable to those of Bi_2Te_3 ¹⁴ or Sb_2Te_3 ¹⁵. The Hall Effect measurement on BiTeI was conducted at high pressure with a magnetic field H perpendicular to the ab plane of the sample up to 5 T at a fixed temperature (30 K) for each given pressure. The samples show n type carrier features in all pressure temperature ranges as shown in Fig. 4.

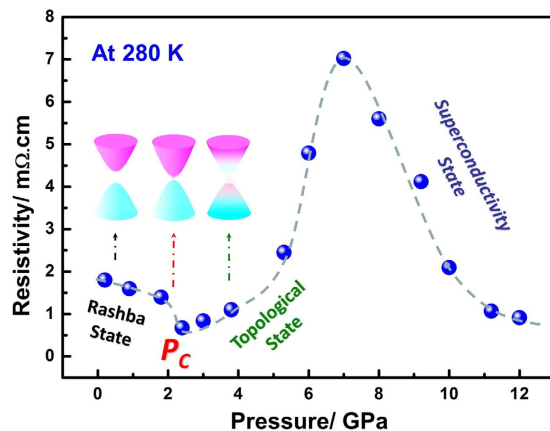


Figure 2. Resistivity of the BiTeI single crystal at 280 K and in the pressure range of 0 GPa to 12 GPa. The transition from the Rashba type topological trivial state to the topological non trivial quantum state at $P_C \sim 2$ GPa is indicated by the minimum resistivity level. Insets show schematics of the energy band inversion across the topological quantum phase transition. Magenta denotes the conduction band, whereas cyan denotes the valence band. At P_C , the surface metallic state was represented by the Dirac Cone, which comes from the inversion of the Bi 6_{pz} orbital and Te/I- $5pz$ orbitals.

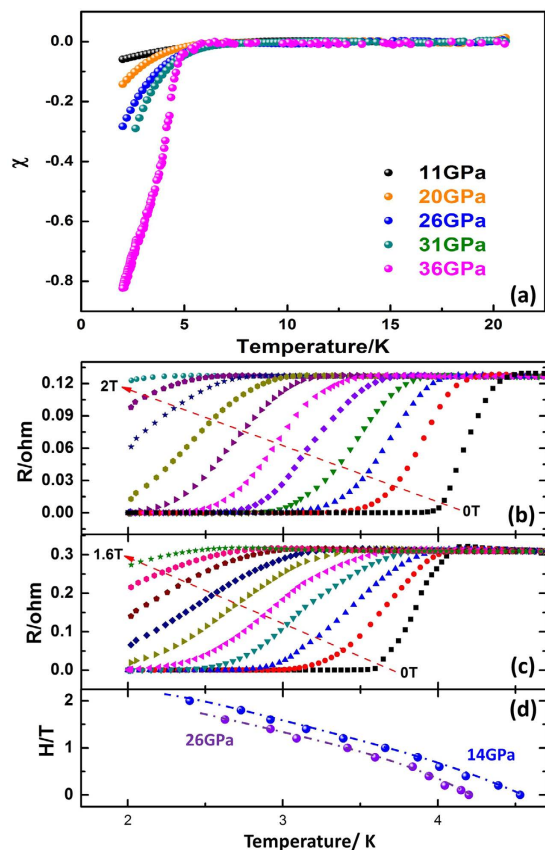


Figure 3. (a) ac magnetic susceptibility of BiTeI as a function of temperature at high pressure; (b,c) Magnetic field dependence of the superconductivity transition of the BiTeI single crystal at 14 GPa and 26 GPa with an applied magnetic field H perpendicular to the ab plane, and (d) the dependence of T_C on the magnetic field H .

Structure evolution of the BiTeI single crystal at high pressures. High pressure synchrotron X-ray diffraction of BiTeI was conducted (Fig. S1a) to trace the origination of the different quantum state transitions considering crystal structural evolutions. Rietveld refinement was performed for the X-ray diffraction patterns, and the refined volumes of all the phases are shown in Fig. S1(b). The first pressure induced structure transition was observed above 10.6 GPa, whereas the second structure transition was observed above 20 GPa as shown in Fig. S1(a).

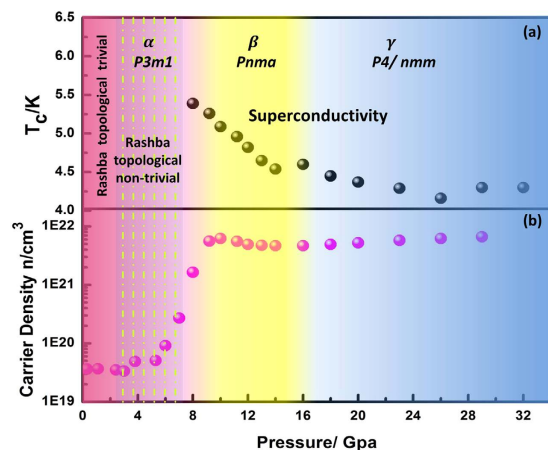


Figure 4. (a) Superconducting transition temperature (T_C) and (b) n type carrier density of the BiTeI single crystal fixed at 30 K as function of pressures. The first superconducting transition appears at ~ 8 GPa, followed by extension into the region above ~ 16 GPa.

Raman spectroscopy was conducted to obtain insights into the local structure evolution at high pressure levels (Fig. S3). The symmetry analysis indicates that BiTeI has four zone center vibrational modes at ambient conditions with the irreducible vibrational representation $\Gamma = 2A_1 + 2E^{19}$. Figure S3(c) shows that: (i) the intensity of the $A_1(1)$ vibrational mode is gradually suppressed and disappears at ~ 4 GPa at ambient phase, which has relevance with the electronic topological transition, although no sufficient theoretical evidence proves this condition; (ii) $A_1(2)$ and $E(2)$ vibrational modes blue shift up to ~ 7.5 GPa, and a new mode M1 at ~ 136 cm^{-1} appeared above ~ 8.9 GPa, which should be the signatures for the first structure transition; (iii) all the three modes become softened above ~ 15.8 GPa, whereas a new mode M2 appeared at ~ 163 cm^{-1} that can be associated with the further high pressure induced structure transition.

The high pressure synchrotron X-ray diffraction and high pressure Raman spectroscopy experiments jointly indicate that the first pressure induced structure transition should be at 7.5 GPa to 8.9 GPa from the hexagonal $P3m1$ (denoted as α BiTeI) ambient phase to the orthorhombic $Pnma$ (denoted as β BiTeI) high pressure phase. The second structure transition should be at 15.8 GPa to 17.2 GPa from the orthorhombic $Pnma$ high pressure phase to the tetragonal $P4/nmm$ (denoted as γ BiTeI) high pressure phase^{13,20}. The coordination of Bi cations is believed to take important role in tracing (tuning) the changes; their schematic views are shown in Fig. S2.

Figure 4 summarizes the global phase diagram of the quantum phase evolution of BiTeI, especially the relationship between the superconductivity temperature T_C (a) and carrier densities (b) as function of pressures. BiTeI is of n type carriers with a carrier density of $3.62 \times 10^{19} \text{ cm}^{-3}$ at ambient pressure as measured from the Hall coefficient similar to that in⁹. The carrier density changes slightly below 6.0 GPa. The carrier density above 6 GPa increases rapidly over three orders of magnitude that reaches approximately $6.23 \times 10^{21} \text{ cm}^{-3}$ at 10 GPa as indicated in Fig. 4(b). Consequently, the superconducting state is accompanied with a sharp increase in the carrier density. The increases in carrier density across phases α to β after the topological trivial to non-trivial transition in the Rashba phase is therefore expected to signal the pressure induced superconductivity. $T_C^{\text{(onset)}}$ decreases with the further pressure increase to 32 GPa.

The previous structure¹⁷ study indicates that a semi-ionic model with polar axis along the atomic stacking direction can be applied to describe the BiTeI structure at ambient phase that consists of a corrugated $(\text{BiTe})^+$ layer and I^- anions; however, Bi-I contacts are considered to be ionic⁹.

To understand the structural related origin of transport properties, we plotted the bond length of Bi-Te and Bi-I, the bond angle of Te~Bi~Te obtained from the Rietveld Refinements based on our experiments in Fig. 5.

Figure 5 shows that in phase α (ambient pressure phase), the bond length of Bi-I decreases with pressure to ~ 2 GPa, then increases sharply with pressure to ~ 8 GPa. The same results are observed for the bond angle of Te~Bi~Te. This scenario causes another V shape change across P_C . The decrease in the Bi-I bond length with pressure to 2 GPa indicates an enhanced band width, which results into a gradual narrowing and closing of the band gap. The increase in these structural parameters with pressure to 8 GPa in turn leads to the gradual reopening of the band gap above 2 GPa. Signatures of V shape change of resistivity from transport measurements shown in Fig. 2 therefore well correlate to the evolution of respective structural parameters.

The BiTeI structure in phase β (high pressure phase 1) consists of positively charged $(\text{BiTe})^+$ ladders, where Bi-Te has weak Bi-Te covalent bonds surrounded by I^- ions¹⁸. The increase in the Bi-Te bond length with pressure can result in more ionic bonds of Bi-Te, which results in less localized behavior of electrons. The decreased bond angle of Te~Bi~Te with pressure compresses the $(\text{BiTe})^+$ ladders along the b-axis and suppresses the band gap. The above structure distortion can contribute to less semiconductive behavior and properly coincides with the resistivity decrease in this phase as shown in Fig. 2. Figure 4 shows that T_C decreases dramatically, whereas the carrier density maintains almost no change in the pressure range from 11 GPa to 20 GPa. This condition is inconsistent with conventional superconductivity, where T_C generally changes as function of carrier density²¹. However, the phonon frequency and electronic density of states $N(E_F)$ can be balanced to control T_C as stated by BCS theory

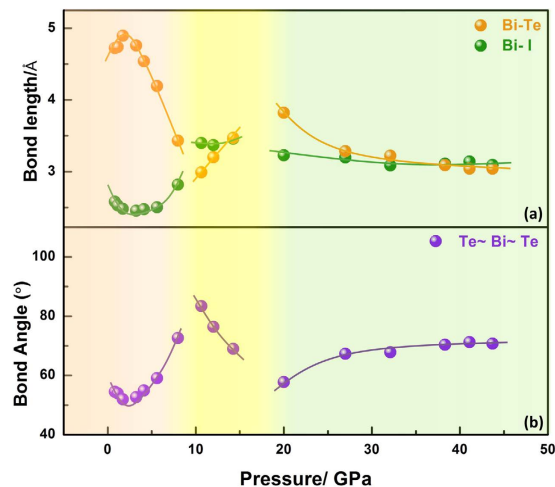


Figure 5. (a,b) Structure parameters about the bond lengths of Bi-Te and Bi-I, as well as the bond angle of Te~Bi~Te.

or the McMillan electron-phonon coupling formalism²². Therefore, anomaly phonon spectrum changes in this pressure range can be expected. The refined bulk modulus B_0 and lattice volume V_0 in phases α and β are comparable as shown in Fig. S1, which indicates that the structure of phase β can preserve a similar lattice property with phase α . Considering that superconductivity emerged at the border across the topological phases α to β , this condition implies that the superconductivity in this pressure range should result from a topological precursor³.

The bond length of the Bi-Te atoms in phase γ (high pressure phase 2) decreases, whereas the Bi-I bond length remains almost constant. The electronic band structure shows that BiTeI in this phase is metallic¹⁸. The T_C in this phase initially decreases when the bond length of the Bi-Te atoms decreases. T_C then increases slightly when the bond lengths of Bi-Te and Bi-I, as well as the Te~Bi~Te bond angle, remain almost non change. These observations indicate that the T_C variation correlates with the structure evolution at pressures. Figure S1b shows that the refined bulk modulus B_0 in phase γ is much larger than that in phase β , whereas the refined V_0 is much smaller than that of phase β , which indicates that the phase γ structure differs from that of phase β . The ac magnetic susceptibility measurement shows that the superconducting volume fraction increases with applied pressure, which signifies that the superconductivity transforms from the surface states at the border range in phases α to β to bulk nature in phase γ .

In summary, we successfully observed pressure induced consecutive transitions for a SOI compound from a Rashba-type topological trivial phase to a topological insulator followed by a classical quantum condensation (i.e., superconductivity). The evolutions properly correlate with the bonding parameter changes of the structures. The observed superconductivity from the topological precursor phase points to a possible unconventional nature.

Methods

The BiTeI single crystals are grown utilizing the Bridgman method. The Te powder, Bi, and I reagents are mixed together at a proper stoichiometric ratio. The mixtures are then grounded thoroughly in an agate mortar to ensure homogeneity. The mixtures are sealed in an evacuated quartz tube under 10^{-4} Pa and heated to 660 °C for 24 h, followed by slow cooling at a rate of 12 °C/h to 100 °C before quenching to room temperature.

The electronic transport properties of BiTeI at a low pressure range (<2 GPa) are measured through four probe electrical conductivity methods in a Piston Cylinder cell made of CuBe alloy. A piece of the BiTeI single crystal with a dimension of 2 mm * 1 mm * 0.15 mm was loaded into a Teflon-made vessel with Daphne oil loaded as the pressure transmitting medium. A manganese copper wire was placed near the sample as a pressure marker. The cell was placed inside a Maglab system with an automatic temperature control model. A semiconductor thermometer was mounted on the surface of the cell to monitor the temperature. The electronic transport properties of BiTeI with pressure higher than 2 GPa are measured through four probe electrical conductivity methods in a diamond anvil cell (DAC) made of CuBe alloy. The diamond culet is 300 μ m in diameter. The Au wires with a diameter of 18 μ m are used as electrodes. A T301 stainless steel gasket was compressed from a thickness of 250 μ m to 40 μ m, and then a hole at 150 μ m in diameter was drilled. The cubic BN applied as an insulating layer was pressed into this hole. A small center hole at 100 μ m in diameter was further drilled to serve as the sample chamber, where NaCl fine powder serves as a pressure transmitting medium and a piece of BiTeI single crystal with dimensions of 90 μ m * 90 μ m * 20 μ m was loaded. A piece of ruby was loaded simultaneously as a pressure marker. The DAC was placed inside a Maglab system with automatic temperature control. A thermometer was mounted near the diamond to monitor the temperature. The high pressure Hall coefficients are measured utilizing the Van der Paul method.

The high pressure Raman experiments are conducted on single crystal BiTeI with dimensions of 60 μ m * 60 μ m * 20 μ m with Renishaw Raman Spectroscopy with a laser wavelength of 532 nm and spectral resolution ~ 1 cm^{-1} in a DAC. Silicon oil was applied as the pressure medium. The diamond culet is 300 μ m in diameter. The T301 stainless steel gasket was compressed from 250 μ m to 40 μ m, and a center hole at 140 μ m in diameter was drilled. A small piece of ruby was placed aside the specimen to measure pressure.

High pressure synchrotron X-ray diffraction experiments are performed at 16 BMD, HPCAT of the Argonne National Laboratory with a wavelength of 0.4246 Å in a symmetric DAC with a culet at 300 μm in diameter. The T301 steel gasket was pre-indented from 300 μm to ~40 μm, and a center hole at 150 μm in diameter was drilled. The hole was compressed to 120 μm with neon loaded as a nearly hydrostatic pressure transmitting medium. Ruby balls are placed near the sample as pressure markers. The X-ray diffraction patterns are collected with a MAR 3450 image plate detector. The obtained 2D image plate patterns are converted to 1D 2θ versus intensity data utilizing the Fit2D software package²³. Refinements of the measured X-ray diffraction patterns are performed by applying the GSAS + EXPGUI software packages^{24,25}.

References

1. Qi, X. L., Hughes, T. L., Raghu, S. & Zhang, S. C. Time-reversal-invariant topological superconductors and superfluids in two and three dimensions. *Phys. Rev. Lett.* **102**, 187001 (2009)
2. Hasan, M. Z. & Kane, C. L. Colloquium: topological insulators. *Rev. Mod. Phys.* **82**, 3045–3067 (2010).
3. Mackenzie, A. P. & Maeno, Y. The superconductivity of Sr₂RuO₄ and the physics of spin-triplet pairing. *Rev. Mod. Phys.* **75**, 657–712 (2003)
4. Cao, G. *et al.* Novel Magnetism of Ir⁵⁺ (5d⁴) Ions in the Double Perovskite Sr₂YrO₆. *Phys. Rev. Lett.* **112**, 056402 (2014).
5. Kitaev, A. Periodic table for topological insulators and superconductors. *AIP Conf. Proc.* **1134**, 22–30 (2009).
6. Schnyder, A. P., Ryu, S., Furusaki, A. & Ludwig, A. W. Classification of topological insulators and superconductors in three spatial dimensions. *Phys. Rev. B* **78**, 195125 (2008).
7. Ryu, S., Schnyder, A. P., Furusaki, A. & Ludwig, A. W. Topological insulators and superconductors: tenfold way and dimensional hierarchy. *New J. Phys.* **12**, 065010 (2010).
8. Fu, L. & Kane, C. L. Superconducting proximity effect and Majorana fermions at the surface of a topological insulator. *Phys. Rev. Lett.* **100**, 096407 (2008).
9. Ishizaka, K. *et al.* Giant Rashba-type spin splitting in bulk BiTeI. *Nat. Mater.* **10**, 521–526 (2011).
10. Bahramy, M. S., Yang, B. J., Arita, R. & Nagaosa, N. Emergence of non-centrosymmetric topological insulating phase in BiTeI under pressure. *Nat. Comms.* **3**, 679 (2012).
11. Datta, S. & Das, B. Electronic analog of the electro-optic modulator. *Appl. Phys. Lett.* **56**, 665–667 (1990).
12. Bauer, E. *et al.* Heavy Fermion Superconductivity and Magnetic Order in Noncentrosymmetric CePt₃Si. *Phys. Rev. Lett.* **92**, 027003 (2004)
13. Xi, X. X. *et al.* Signatures of a pressure-induced topological quantum phase transition in BiTeI. *Phys. Rev. Lett.* **111**, 155701, (2013).
14. Zhang, J. L. *et al.* Pressure-induced superconductivity in topological parent compound Bi₂Te₃. *Proc. Natl. Acad. Sci.* **108**, 24–28 (2011).
15. Zhu, J. *et al.* Superconductivity in topological insulator Sb₂Te₃ induced by pressure. *Sci. Rep.* **3**, 2016 (2013).
16. Kong, P. P. *et al.* Superconductivity of the topological insulator Bi₂Se₃ at high pressure. *J. Phys. Condens. Matter.* **25**, 362204 (2013).
17. Shevelkov, A. V., Dikarev, E. V., Shpanchenko, R. V. & Popovkin, B. A. Crystal structures of bismuth tellurohalides BiTeX (X = Cl, Br, I) from X-ray powder diffraction data. *Journal of Solid State Chemistry.* **114**, 379–384 (1995).
18. Werthamer, N. R., Helfand, E. & Hohenberg, P. C. Temperature and purity dependence of the superconducting critical field, H_{c2} . III. electron spin and spin-orbit effects. *Phys. Rev.* **147**, 295–302 (1966).
19. Tran, M. K. *et al.* Infrared-and Raman-spectroscopy measurements of a transition in the crystal structure and a closing of the energy gap of BiTeI under pressure. *Phys. Rev. Lett.* **112**, 047402 (2014).
20. Chen, Y. Z. *et al.* High-pressure phase transitions and structures of topological insulator BiTeI. *J. Phys. Chem. C* **117**, 25677–25683 (2013).
21. Allen, P. B. & Cohen, M. L. Carrier-concentration-dependent superconductivity in SnTe and GeTe. *Phys. Rev.* **177**, 704 (1969).
22. Schilling, J. S. Handbook of High-Temperature Superconductivity (eds Schrieffer, J. R., assoc eds Brooks, J. S.) Ch. 11, High-Pressure Effects, 430–433 (Springer, 2007).
23. Hammersley, A. P., Svensson, S. O., Hanfland, M., Fitch, A. N. & Hausermann, D. Two-dimensional detector software: from real detector to idealised image or two-theta scan. *High. Pres. Res.* **14**, 235–248 (1996).
24. Larson, A. C. & Von Dreele, R. B. GSAS-General Structure Analysis System. *Los Alamos National Laboratory Report LAUR*. 86–748 (2000).
25. Toby, B. H. E. X. P. G. U. I. a graphical user interface for GSAS. *J. Appl. Crystallogr.* **34**, 210–213 (2001).

Acknowledgements

The work was supported by NSF & MOST of China through research projects. HPCAT operations are supported by DOE-NNSA under Award No. DE-NA0001974 and DOE-BES under Award No. DE-FG02-99ER45775, with partial instrumentation funding by NSF. APS is supported by DOE-BES, under Contract No. DE-AC02-06CH11357.

Author Contributions

C.Q.J. conceived research; M.L.J. conducted the high pressure measurements with assistance from S.J.Z., S.M.F., W.M.L.; L.Y.X. synthesized the sample with help of X.C.W.; F.S. is responsible for the high pressure XRD experiment at supervision of W.G.Y., G.Y.S. & H.K.M.; M.L.J. analyzed the data with help of C.Q.J., J.L.Z., R.C.Y. & Y.S.Z.; J.M.L. & C.Q.J. wrote the paper with the comments of Y.W.L., H.Y.B., C.Z.G.; All authors discussed the results and commented on the manuscript.

Additional Information

Supplementary information accompanies this paper at <http://www.nature.com/srep>

Competing financial interests: The authors declare no competing financial interests.

How to cite this article: Jin, M.L. *et al.* Superconductivity Bordering Rashba Type Topological Transition. *Sci. Rep.* **7**, 39699; doi: 10.1038/srep39699 (2017).

Publisher's note: Springer Nature remains neutral with regard to jurisdictional claims in published maps and institutional affiliations.



This work is licensed under a Creative Commons Attribution 4.0 International License. The images or other third party material in this article are included in the article's Creative Commons license, unless indicated otherwise in the credit line; if the material is not included under the Creative Commons license, users will need to obtain permission from the license holder to reproduce the material. To view a copy of this license, visit <http://creativecommons.org/licenses/by/4.0/>

© The Author(s) 2017